

# Silica Supraparticles with Self-Oscillatory Vertical Propulsion: Mechanism & Theoretical Description

Hyung-Ju Kim, Marcel Sperling, Orlin D. Velev,\* and Michael Gradzielski\*

A novel type of mm-sized silica-based self-propelling supraparticles displaying buoyancy-driven homogeneous vertical oscillatory motion using aqueous hydrogen peroxide ( $\text{H}_2\text{O}_2$ ) as chemical fuel is presented. The supraparticles are prepared via a robust droplet templating technique by drying colloidal suspension droplets containing silica microspheres and catalytic  $\text{Fe}_3\text{O}_4$ @Pt decorated nanoparticles on a superhydrophobic Cu–Ag surface. Oxygen gas originating from Pt catalyzed decomposition of  $\text{H}_2\text{O}_2$  is released and gathered onto the hydrophobic supraparticle surface. This causes buoyancy and uplift of the particle to the surface, where the oxygen bubble is released and the particle descends again, leading to an oscillating process in a very regular fashion. The mechanism of this process is characterized and analyzed here quantitatively by a balance of the gravitational and buoyant forces. The theoretical model of particle movement describes how the particle oscillation period depends on the  $\text{H}_2\text{O}_2$  concentration. This novel type of self-propelling particles could find potential applications in mixing and catalysis, especially due to the high regularity of their periodic movement.

creation of many new types of functional materials.<sup>[2]</sup> This functionality can for example be of structural, optical, or chemical nature. Sperling et al. have shown that the use of fumed silica as colloidal building block assembled inside aqueous droplets residing on superhydrophobic surfaces results in the formation of anisometric supraparticles possessing boat-like shape,<sup>[3]</sup> where those particles can also enclose additional colloids.<sup>[4]</sup> Besides shape, internal structuring of such particles can be achieved by forming patchy assemblies by the use of polystyrene microspheres and highly light-diffracting gold nanoparticles<sup>[1]</sup> or magnetic particles.<sup>[5]</sup> The latter furthermore allows for defined patch positioning in supraparticles with anisometric ellipsoidal shape by using bent superhydrophobic surfaces.<sup>[6]</sup> The technique of droplet templating on superhydrophobic surfaces,<sup>[7]</sup> thus allows for

## 1. Introduction

The fabrication of colloidal supraparticles by use of the suspension droplet templating technique on solid superhydrophobic surfaces<sup>[1]</sup> has proven to provide a powerful tool for the

efficient formation of isotropic and anisotropic supraparticles, which in turn offer high potential for applications in the field of self-propelling devices.<sup>[8–10]</sup>

Self-propelling particles harvest energy from their media to generate a force for movement by consumption of a chemical fuel via a usually anisometrically distributed catalyst.<sup>[11]</sup> The most popular chemical “fuel” is hydrogen peroxide ( $\text{H}_2\text{O}_2$ ), when using metals, such as Pt or Pd as a catalyst.<sup>[12]</sup> Many particles of this kind published in literature are of spherical shape,<sup>[13,14]</sup> although rod-like particles have also been extensively studied and several modes of movement have been proposed. In general, such particles mostly consist of two or three metals such as Au and Pt, Ni, or Pd as a catalyst<sup>[15]</sup> and are asymmetric in architecture, i.e., are of Janus type. This type of particles driven by  $\text{H}_2\text{O}_2$  decomposition are for instance used for targeted delivery of species and the rate of movement can be controlled by the  $\text{H}_2\text{O}_2$  concentration.<sup>[16]</sup> Furthermore, the particle velocity can be controlled by the solution pH<sup>[17]</sup> and as the decomposition reaction proceeds at the interface it can be modified by the presence of surfactants.<sup>[18]</sup> In addition to metal catalysts, one may also employ enzymes or catalysts mimicking them, like synthetic manganese catalase.<sup>[19]</sup> During  $\text{H}_2\text{O}_2$  decomposition, oxygen bubbles are formed on the particle surface, where buoyancy can lead to vertical motion,<sup>[20]</sup> while the typically mainly observed horizontal motion is likely to be explained by the detachment mechanism of the oxygen bubbles.<sup>[14]</sup> A recent investigation has shown that in addition to the overall shape of the particles also the nanometric details of the catalyst play an important role.<sup>[21]</sup>

H.-J. Kim, O. D. Velev  
Department of Chemical & Biomolecular Engineering, 911 Partners Way  
North Carolina State University  
Raleigh NC 27695-7905, USA  
E-mail: odvelev@ncsu.edu

H.-J. Kim  
Decommissioning Technology Research Division  
Korea Atomic Energy Research Institute  
989-111 Daedeok-daero, Yuseong-gu, Daejeon 34057, Republic of Korea

M. Sperling, M. Gradzielski  
Institut für Chemie - Stranski Laboratorium für Physikalische  
und Theoretische Chemie  
Technische Universität Berlin  
Straße des 17. Juni 124, D-10623 Berlin, Germany  
E-mail: michael.gradzielski@tu-berlin.de

 The ORCID identification number(s) for the author(s) of this article can be found under <https://doi.org/10.1002/ppsc.202200021>.

© 2022 The Authors. Particle & Particle Systems Characterization published by Wiley-VCH GmbH. This is an open access article under the terms of the Creative Commons Attribution License, which permits use, distribution and reproduction in any medium, provided the original work is properly cited.

DOI: 10.1002/ppsc.202200021

The use of toxic  $\text{H}_2\text{O}_2$  restricts the applicability of such systems, but other chemical reactions like the oxidation of primary alcohols can be employed in powering active motile systems.<sup>[22]</sup> Moreover, other mechanisms of movement are possible, including bubble propulsion,<sup>[23]</sup> gravitational,<sup>[20]</sup> and Brownian ratchet mechanism,<sup>[24]</sup> self-diffusiophoresis,<sup>[25]</sup> as well as interfacial gradient,<sup>[26]</sup> light driven<sup>[27]</sup> or electrokinetically driven mechanisms.<sup>[28,29]</sup>

In general, the design of self-propelling devices plays an important role with respect to mechanism and direction of movement, but also to programmed guiding, involving patterning,<sup>[30]</sup> chemical fuel gradient,<sup>[31]</sup> or magnetic manipulation,<sup>[32]</sup> which offer possibilities to effectively influence particle trajectories. Sundararajan et al. reported the dynamics of Au-Pt bimetallic nanorods of  $\approx 1.5 \mu\text{m}$  length and  $\approx 0.4 \mu\text{m}$  diameter.<sup>[33]</sup> They have been able to use this device to transport polystyrene microspheres as small cargo, bound via electrostatic or chemical interaction, along a concentration gradient of  $\text{H}_2\text{O}_2$ . Adding magnetic Ni to the rods also showed stabilization of the particle trajectory in terms of orientation under the action of an applied external magnetic field. Similar means of cargo transport have been reported by Burdick et al. using magnetic interaction for reversible binding.<sup>[34]</sup> A micro-submarine having superhydrophobic surface coating could be able to collect oil droplets navigating.<sup>[35]</sup>

Most of the autonomously moving particles reported in literature to date are capable of horizontal 2D translation. One example for vertical motion was published recently by Campbell and Ebbens, who used gravitation to orient the direction of motion particles with a diameter of  $3 \mu\text{m}$  or larger via anisotropic metal coating.<sup>[36]</sup> In another example,  $2 \mu\text{m}$  sized silica particles were converted to Janus particles with a Pt coverage on one half of the particle. These Janus particles were moving on the surface of an aqueous solution due to the decomposition of  $\text{H}_2\text{O}_2$ . Their trajectories on the surface have been largely controlled by the  $\text{H}_2\text{O}_2$  concentration.<sup>[37]</sup> Referring to particle size, most studied particles are in the  $\mu\text{m}$  size range and to date there are few publications dealing with bigger self-propelling particles. Working with larger particles, Dey et al. used a fuel gradient induced by pH to guide a vertical movement trajectory, where particles used in this case were of about  $0.7 \text{ mm}$  size.<sup>[31]</sup> A novel, soft type of self-propelling gel-based particle in the size range of several mm was reported by Sharma et al., who used ethanol infused hydrogel to promote dancing movement driven by the Marangoni effect.<sup>[38]</sup>

In this paper, we describe a new type of autonomously moving supraparticle in the sub-mm size range performing oscillating vertical motion or elevation, by means of oxygen bubble growth via Pt catalyzed decomposition of aqueous  $\text{H}_2\text{O}_2$  and subsequent bubble release at the air-water interface based on recently reported experimental observation by ourselves.<sup>[39]</sup> These supraparticles are prepared via the droplet templating method,<sup>[40]</sup> by deposition of colloidal suspension droplets on a superhydrophobic surface and subsequent drying. We provide a full analysis of the movement mechanism and give a simple physical model, that accounts for the observations at different fuel, here  $\text{H}_2\text{O}_2$ , concentrations. By correlating to the reaction kinetics, we apply our model to the experimentally

observed oscillation time dependence of the particle movement depending on  $\text{H}_2\text{O}_2$  concentration. A full explanation of our concept is given and the model strengths and limitations in terms of prediction capability are discussed.

## 2. Mechanism and Theoretical Description

### 2.1. Experimental Observation

We recently reported a new type of self-propelling supraparticles performing oscillatory vertical motion similar to that of an elevator.<sup>[39]</sup> This type of motion is promoted by catalytic oxygen production by Pt catalyzed decomposition of  $\text{H}_2\text{O}_2$ , described in Equation (1).



The produced oxygen gathers into bubbles attached to the supraparticle surface, due to the surface hydrophobicity tailored during particle preparation (see Experimental section), as shown in **Figure 1a**. While the particle surface is covered with several small bubbles, one big bubble mainly responsible for buoyancy is formed, as shown in **Figure 1b**. Oxygen is continuously generated catalytically, and the bubble grows until it creates enough buoyancy to begin lifting the particle to the top of the container (**Figure 1c**). Here the bubble gets released into the air layer between the hydrophobic Teflon surface and liquid interface (**Figure 1d**). This is followed by the particle descending by gravity towards the bottom and then a new movement cycle starts, because of the continued production of  $\text{O}_2$ . This oscillating movement will then be repeated in a very regular fashion for extended periods of time (up to several days by our observation). We analyze here the origins of this movement and the means to control it.

The oscillation time (or cycle frequency) depends on the initial concentration of  $\text{H}_2\text{O}_2$  in the aqueous phase. In our experiments, this effect was analyzed by tracking of the particle position over time. From the video files, we extracted the height function,  $h(t)$ , and derived from that velocity,  $v(t)$ , and acceleration,  $a(t)$ , for details see Supporting Information. Some example curves for  $h(t)$ ,  $v(t)$ , and  $a(t)$  are given in **Figure 2** for 0.5, 5, and 20 wt% aqueous  $\text{H}_2\text{O}_2$  solutions. For low  $\text{H}_2\text{O}_2$  concentration,

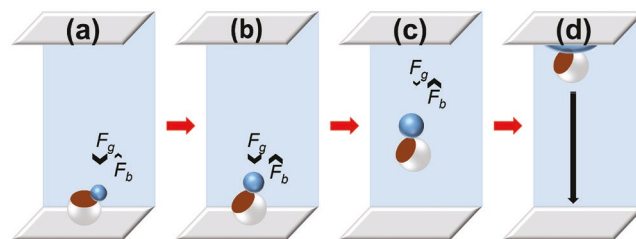


**Figure 1.** Mechanism of particle movement. a) Particle located on Teflon bottom generating oxygen gas forming a bubble attached at the particle surface. Gravity ( $F_g$ ) is still larger than buoyancy ( $F_b$ ),  $F_g > F_b$ ; b)  $F_b$  equals to  $F_g$  tilting the particle,  $F_g \approx F_b$ . c) Particle is lifted to the top due to further increasing  $F_b$ ,  $F_g < F_b$ . d) Bubble is detached at the Teflon top and the particle descends to bottom.

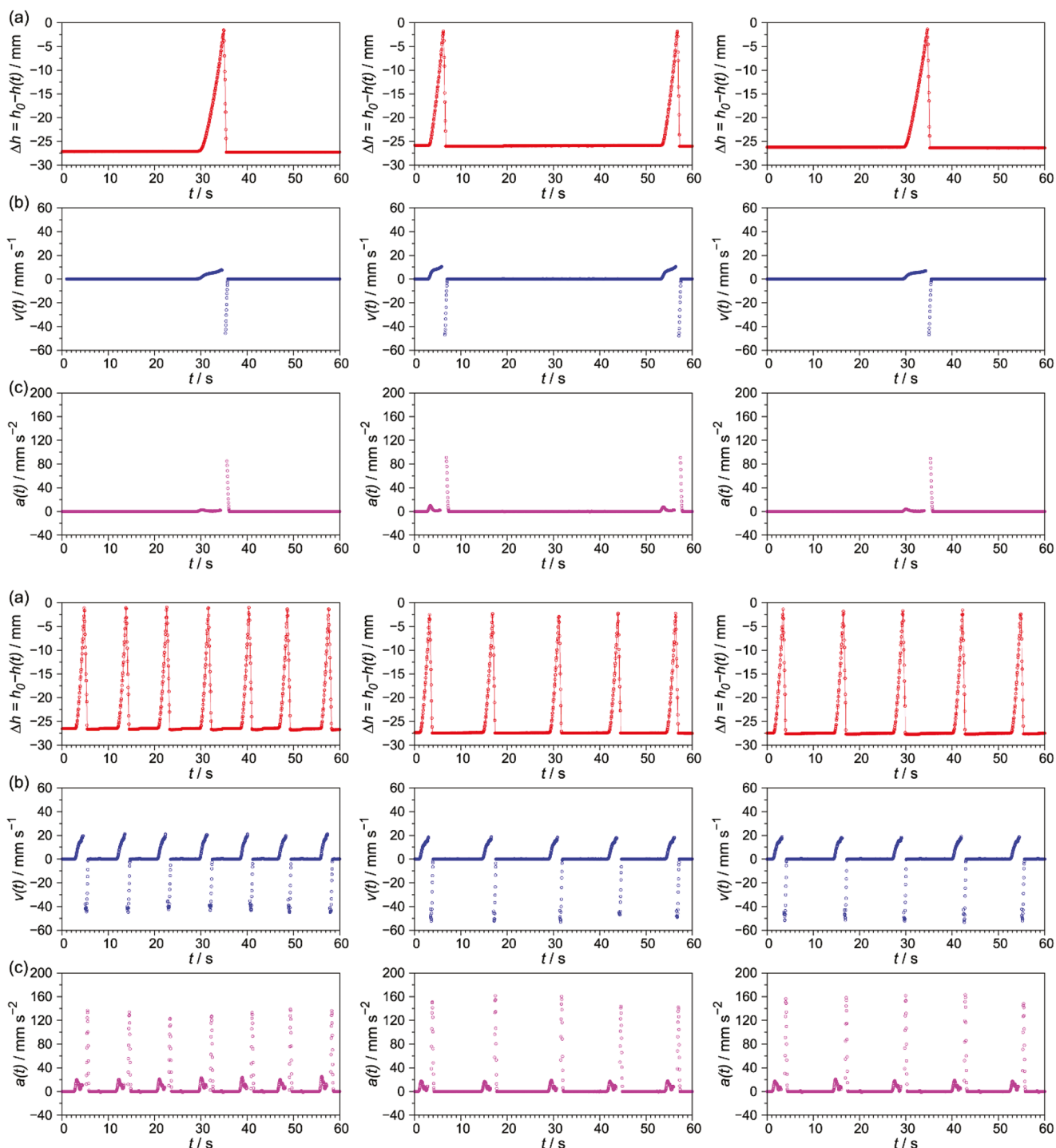


**Figure 2.** Plots of a)  $h(t)$ , b) first derivative  $v(t)$ , and c) second derivative  $a(t)$  for three particles. Top: 0.5 wt%  $\text{H}_2\text{O}_2$ ; middle: 5 wt%  $\text{H}_2\text{O}_2$ ; bottom: 20 wt%  $\text{H}_2\text{O}_2$ .

the particles drop to the bottom ( $\Delta h = -27$  mm), while for high concentration of 15–20 wt% the particles already revert their motion before hitting the bottom, thereby performing a fully oscillatory movement. In general, one observes a very regular movement and one that is well reproduced as shown here for 3 different particle trackings.

## 2.2. Theoretical Description

The description of the elevator particle movement, in terms of velocity  $v_{el}$ , can be done by Newton's second law (Equation 2), by balancing the forces affecting it. For simplification, the mass of the elevator particle  $m_{el}$ , was taken as constant, as the increase

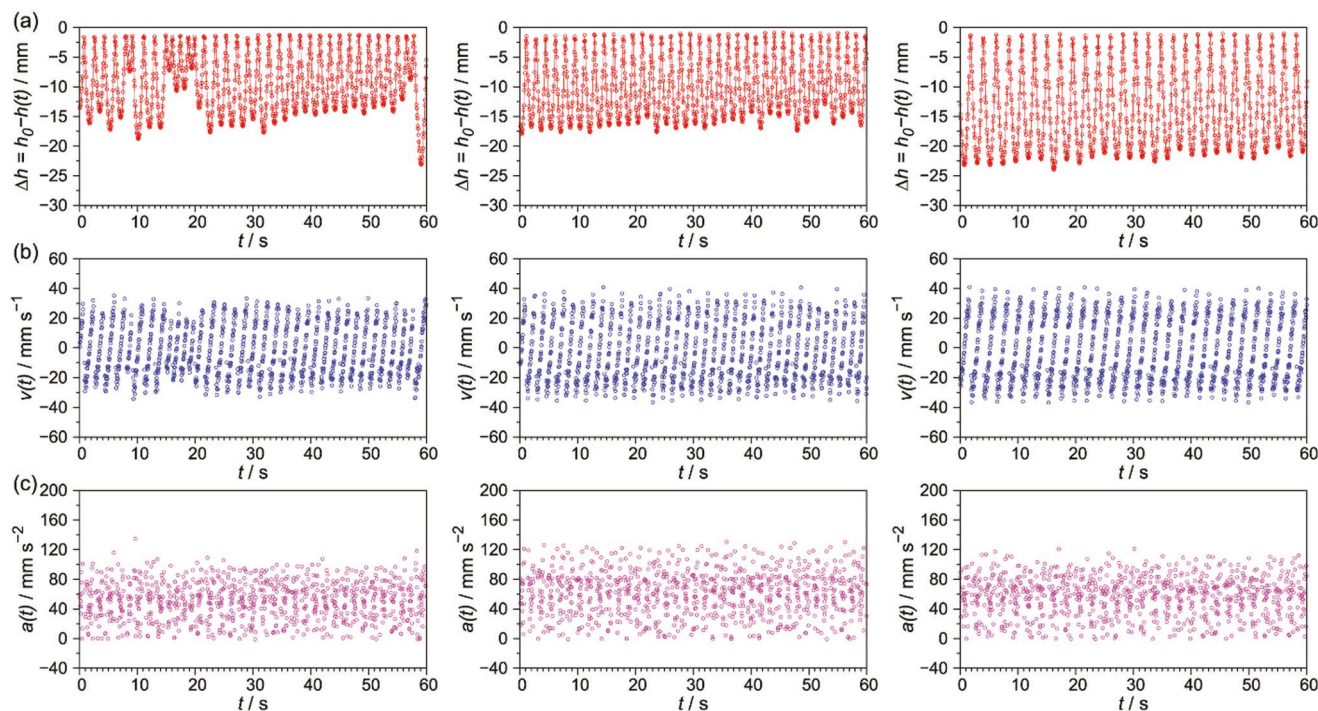


Figure 2. continued.

of mass arising from the growing gas bubble is small. The relevant forces  $F_i$  associated within this process are gravity ( $F_g$ ), buoyancy ( $F_b$ ), and friction ( $F_{fr}$ ), and all of them change with time. With Equation (2), we only consider movement in the z-direction, as any forces operating in other directions should be negligible and the small extent of lateral movement was also validated experimentally as shown in Figure S1 (Supporting Information). The sign in front of  $(F_g - F_b)$  will depend on the direction of movement, being positive for upward motion and negative for downward motion.

$$m_{el} \cdot \dot{v}_{el}(t) = \pm(F_g(t) - F_b(t)) - F_{fr}(t) \quad (2)$$

The  $F_g(t)$  and  $F_b(t)$  are given as Equations S1 and S2 (Supporting Information) with a comprehensive description of relevant parameters in detailed theoretical description (Supporting Information). Also,  $F_{fr}(t)$  in a solvent of viscosity  $\eta$  was simply approximated by the Stokes equation (Equation S3, Supporting Information). This is a valid assumption as the particles are moving under laminar flow conditions, since the dimensionless Reynolds number ( $Re$  in Equation (3) where  $\rho_{sol}$  is density of solvent,  $r_{el}$  is radius and  $v_{el}$  is velocity of the particle), will be less than 40, as even for the highest  $H_2O_2$  concentration of 20 wt% the maximum velocity (see Figure 2 bottom) is below  $40 \text{ mm s}^{-1}$  (for further details of  $Re$  calculation see also Table S1, Supporting Information).

$$Re = \frac{\rho_{sol} r_{el} v_{el}}{\eta} \quad (3)$$

Tumbling of the particles could be another issue of concern for describing the particle motion. For homogenous

spheres (the density distribution in our supraparticles may well be approximated to be homogenous) the dimensionless moment of inertia (which is relevant for rotational motion) would be about one, accordingly the moment of inertia of the particles could be relevant.<sup>[41]</sup> However, experimentally we did not observe that tumbling of particles had any significant effect on the particle movement, different to rising spheres of varying density, which may exhibit complex motion.<sup>[42]</sup> However, in our case the particle movement is dominated by moving in z-direction and lateral motion, that could for instance arise from convection, obviously can be neglected (Figure S1, Supporting Information). In summary, apparently, the translational inertia and being well under conditions of laminar flow stabilizes the linear motion of the particles.

For our case of a gas, produced and attached as a bubble onto the particle, a dynamic force equilibrium builds up, leading to oscillatory motion. This motion, depending on the height of the vessel, may take place in two basic modes (1) reversing the direction of its movement during the fall (full oscillation) or (2) the case, where it drops all the way to the bottom of the vessel and rests there until enough oxygen has been produced to start the up-lift again (semi oscillation), shown in Figure 3. It is generally possible to identify the trajectory minimum with  $v_{el} = 0$  for fully oscillating motion. For the case of semi oscillating motion that point is equal to a force equilibrium on the right-hand side of Equation (2) being 0 and at this point in time,  $\Delta t_{rise,s}$ , the elevating motion will begin. The simple mechanical models for each particle motion are described in detailed theoretical description (Supporting Information) based on the well-known first-order reaction of  $H_2O_2$  decomposition.<sup>[43]</sup>

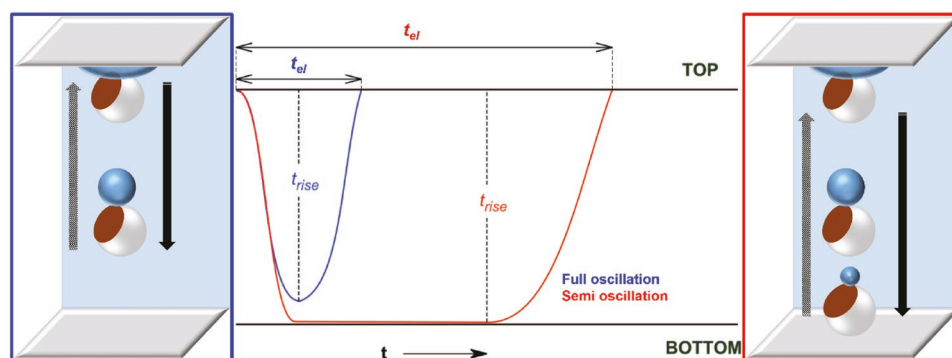


**Figure 3.** Schematics of the time evolution of the full and semi oscillating motion;  $t_{rise}/t_{el}$  converges toward 1 for long oscillation intervals and 0 for shorter intervals.

### 3. Discussion

#### 3.1. Model Application to Experimental Data

In the following, we want to compare our experimental data to this just described model. In order to do so, an appropriate expression for  $\rho_{sol}$  needs to be found. According to Easton et al., the solvent density of aqueous solutions of  $H_2O_2$  at 25 °C, for  $c_0$  in [wt%],  $\rho_{sol}$  in [ $kg\ m^{-3}$ ] is given as:<sup>[44]</sup>

$$\rho_{sol} = 997.0 + 3.4672c_0 + 6.995 \cdot 10^{-3} c_0^2 + 2.885 \cdot 10^{-5} c_0^3 \quad (4)$$

Experimentally, we then determined  $\dot{a}$  for different concentrations  $c_0$  and using the density given by Equation (4) determined the rate constant of  $H_2O_2$  decomposition. As  $\chi$  depends also on  $\rho_{sol}$  (Equation S6b, Supporting Information), it is convenient to rewrite the dependence as:

$$\dot{a} = -\chi \bar{k} c_0 \quad (5a)$$

$$\bar{k} = \frac{gM_{O_2}}{m_{el}} k' \quad (5b)$$

Equation (5b) refers  $k'$  to  $\bar{k}$ , which can be combined with Equation S19 (Supporting Information). With this the experimental data for  $\dot{a}$  are well approximated, as shown in Figure 4, from which one can deduce a value of  $(1.63 \pm 0.05) \times 10^{-5} m\ s^{-3}$  for  $\bar{k}$ . This rate constant describing the decomposition of  $H_2O_2$  then also can be used to calculate the overall expression for the experimentally observed oscillation period,  $\Delta t_{el}$  (shown in Figure 3 and given by Equations S4, S5, S7, S10, and S12, Supporting Information). The required radius  $r_{el}$  of the elevator supraparticles was calculated using the spherical Random-closed-packed geometry with a packing factor of  $\xi = 0.64$ :

$$r_{el} = \left( \frac{3V_{stock}}{4\pi\xi} \sum_i C_{i,vol} \right)^{\frac{1}{3}} \quad (6)$$

The resulting fit to the experimental data as a function of the  $H_2O_2$  concentration is shown in Figure 5, where it must be noted that basically all parameters are known and fixed here by the composition of supraparticles and the experimentally determined decomposition rate of  $H_2O_2$ . The only adjustable

parameter is the amount of permanently adsorbed oxygen, given by  $\beta$  in Equation S1b (Supporting Information). In our case, it turns out to be 0.96, which means that interestingly the volume of permanently bound oxygen, presumably present in pores of the supraparticles, or strongly bound to the surface, is about identical to the dry volume of the colloidal material of the particles.

It is clearly visible that the model describes well the oscillation time dependency up to 15 wt% of  $H_2O_2$ . Above this concentration, however, the model predicts a slightly lower oscillation time than observed in the experiments reported earlier. This may be related to transition in the reaction kinetics to conditions, where the Pt becomes saturated and at this point the reaction converts into zero order kinetics, which subsequently leads to constant particle frequencies. Here Equation S16 (Supporting Information) is no longer valid. This saturation point is not only determined by the pure surface area of the Pt catalyst, but the wettability also plays an important role due to the hydrophobic supraparticle surface. In addition, it should be noted that the amount of oxygen loss from the particle surface may significantly increase at such high concentrations of  $H_2O_2$ . This again results into pseudo-zero-order kinetics as the ability of the hydrophobic surface to retain the produced oxygen is limited, which is not accounted for by our model.

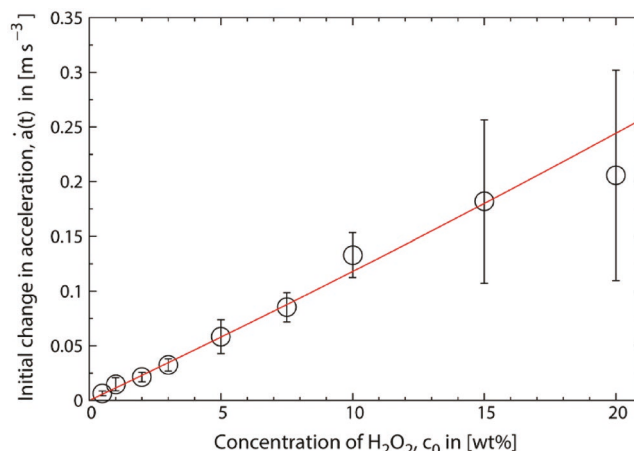


**Figure 4.** Extraction of initial slopes  $\dot{a}$  according to Equation (5a);  $\bar{k}$  gives a value of  $(1.63 \pm 0.05) \times 10^{-5} m\ s^{-3}$ , corresponding to a value of  $3.12 \times 10^{-11} s^{-1}$  for  $k'$ .

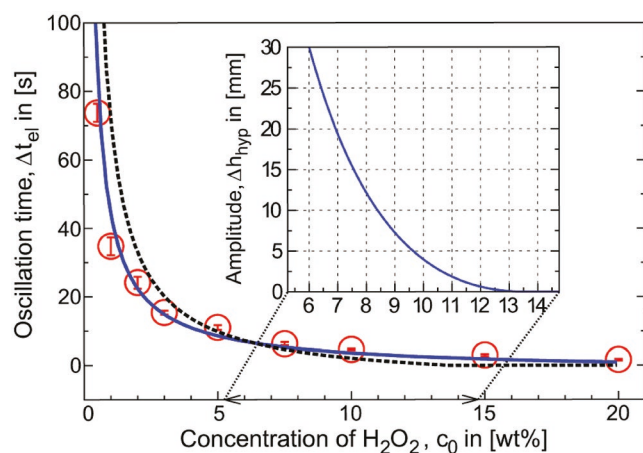


**Figure 5.** Fit of experimental data for elevation time intervals  $\Delta t_{ei}$  based on Equation S4 (Supporting Information) as function of the initial concentration of  $\text{H}_2\text{O}_2$ . There is good correlation between the nonlinearly increasing frequencies with increasing concentration of  $\text{H}_2\text{O}_2$ ; The  $\beta$  values (Equation S1b, Supporting Information) show correlation indicating an approximate constantly collected amount of oxygen equal to 95% to 97% of the total ingredients volume. The black dashed curve shows hypothetical oscillation time for a free particle oscillation without any limitation due to the vessel geometry. The inset shows the expected amplitudes for the hypothetical oscillation between 5.75–14.75 wt% of  $\text{H}_2\text{O}_2$ .

We have also added the hypothetical oscillation time  $\Delta t_{hyp}$  ( $= \Delta t_{rise,f} + \Delta t_{up}$ ) as black dashed curve in Figure 5, as it would be observed for an infinitely deep vessel, i.e., where one has only full oscillation motion even if the concentration of  $\text{H}_2\text{O}_2$  is not high enough. Clearly as a result, the expected elevation time increases compared to the experimental values, as one has the additional travel time of the elevator particle, arising from a larger amplitude. The corresponding hypothetical amplitude  $\Delta h_{hyp}$  is calculated based on  $\Delta t_{hyp}$  and given in the inset of Figure 5. From it, one can see that at  $\approx 6.25$  wt% of  $\text{H}_2\text{O}_2$ , the expected amplitude reaches 27 mm, which equals the experimental liquid/vessel height. This coincides well with the experimental observation of transition from semi to full oscillation mode when approaching higher concentrations (see Figure 2). However, the expected values for  $\Delta t_{hyp}$  and  $\Delta h_{hyp}$  approach 0, when exceeding  $\approx 14$  wt%. This refers to the oxygen production expected at its full retention by the supraparticle being high enough to prevent any sinking and therefore oscillation. The rationale behind this conclusion is again lowered retention of oxygen as increasing concentration of  $\text{H}_2\text{O}_2$  causing higher violent bubble production.

#### 4. Discussion and Conclusions

We present a full mechanical description of the dynamics of a new type of self-propelling supraparticles performing vertical elevating motion by decomposition of  $\text{H}_2\text{O}_2$  in aqueous media as chemical fuel. Upward movement arises from binding of a formed oxygen gas bubble to the hydrophobic supraparticle surface. This oxygen becomes released when the particle reaches the air/water interface, where the bubble breaks through and the supraparticles loses its buoyancy, thereupon

beginning a downward motion that eventually becomes stopped by reforming an oxygen bubble. The resulting oscillating motion is characterized by a very regular oscillation interval, which depends strongly on  $\text{H}_2\text{O}_2$  concentration. A simple model describing this dependency was derived by balancing buoyancy against gravity, while taking into account solvent density, reaction kinetics, friction, and amount to oxygen collected on the supraparticle structure. The volumetric ratio of oxygen generated was evaluated to be around 80–85% comparing to the colloidal volume. This constant adsorption of oxygen onto the supraparticle can be explained by the hydrophobicity of the particle surface and has been validated by optical microscopy. The simple model applies very well below 15 wt% of  $\text{H}_2\text{O}_2$ , while at higher concentrations deviations are seen due to a change in reaction kinetics and limitations of oxygen adsorption on the particle surface. The cycle frequency can be controlled precisely by the concentration of the solution and the overall mass of the particle. The results show how the elevating particle movement can be calculated precisely by a model based on simple physical principles, which therefore can provide useful predictions of particle frequency depending on applied chemical fuel and amount of colloidal ingredients during particle synthesis.

Supraparticles of this type are promising for applications where a chemical system needs mixing, catalytic processing, capturing of dispersed components, or other types of convective transport operations. This is made possible by the simple and robust means of making and actuating these supraparticles. The theoretical expressions for the dynamics of such supraparticles may enable the future fabrication of new smart materials with potential use in catalytic or separation applications, where the very regular and controlled motion of these particles can intensify and enhance the process.

#### 5. Experimental Section

**Preparation of Superhydrophobic Surfaces:** Superhydrophobic Cu–Ag surfaces were prepared according to a procedure reported by Gu et al. using an electrochemical deposition process.<sup>[45]</sup> Polished Cu surfaces were immersed into an aqueous solution containing 0.01 M  $\text{AgNO}_3$  under moderate stirring for 25 min at room temperature. The surface was then dried at ambient conditions and immersed in 0.001 M 1-dodecanethiol dissolved in ethanol for 20 h without stirring. The as-prepared surfaces showed a water contact angle higher than  $150^\circ$  and were operating consistently for several weeks.

**Catalytic Particles—Magnetite Synthesis:** Magnetic  $\text{Fe}_3\text{O}_4$  nanoparticles with a core of 8–15 nm were synthesized according to Kang et al. using a simple coprecipitation method at high pH.<sup>[46]</sup> In a typical synthesis, 2.1 mL of a solution containing 0.617 M  $\text{FeCl}_2$  and 1.234 M  $\text{FeCl}_3$  (molar ratio = 2:1) at 0.4 M HCl was added drop-wise to 20.3 mL of 1.5 M NaOH under vigorous stirring at room temperature. After addition, the particles were collected by means of external magnetic field and washed three times with MilliQ water using centrifugal sedimentation at 2300 g. In a last washing step, the resulting precipitate was refilled with 0.01 M HCl solution and concentrated to a concentration of 0.66 wt% as measured with inductively coupled plasma-optical emission spectrometry (ICP-OES) after having dissolved the particles with aqua regia.

**Catalytic Particles—Pt Decoration:** The resulting magnetite core particles were decorated with Pt in a second step using  $\text{H}_2\text{PtCl}_6$  as precursor and  $\text{NaBH}_4$  as reduction agent. A mass-ratio of 1:10 Pt to  $\text{Fe}_3\text{O}_4$  during synthesis was maintained. For the reaction in aqueous media, a solution of 6 mg  $\text{H}_2\text{PtCl}_6 \times 6\text{H}_2\text{O}$  in 0.2  $\mu\text{L}$  was added quickly to

a suspension of 97 mL volume containing 20 mg  $\text{Fe}_3\text{O}_4$  under vigorous stirring using an Ultra-Turrax at 24 000 rpm. After 2 min of stirring, 1.5 mL of an ice-chilled solution of 0.6 mg  $\text{NaBH}_4$  was added drop-wise at a rate of  $1 \text{ mL min}^{-1}$ . The mixture was allowed to homogenize for another 2 min and then a 1 mL solution of 127 mg Na-citrate dihydrate was added. After additional 3 min of stirring, the resulting particles were cleaned in analogy to the magnetite preparation described in Section 5.2. except for the last HCl washing step. The final suspension had a concentration of 0.46 wt% measured by ICP-OES after microwave-aided decomposition of the particle in aqua regia at  $160 \text{ }^\circ\text{C}$  and 18 bar pressure. The particles showed an average size of about 8–15 nm in diameter based on transmission electron microscopy measurement.<sup>[39]</sup>

**Synthesis of Self-Propelling Elevator Supraparticles:** The “elevator” supraparticles were prepared using the droplet templating method<sup>[3,39]</sup> by deposition of aqueous colloidal suspension droplets under controlled conditions onto a superhydrophobic Cu–Ag surface. For a typical preparation, 3  $\mu\text{L}$  of a suspension containing 10% vol/vol silica (Bangs Laboratories Inc., 780 nm in diameter) and 0.11% vol/vol of catalyst particles (0.0034% vol/vol Pt) were applied, described in Section 5.2. onto the superhydrophobic surface inside a chamber, where the humidity was set to 5–20% using a silica gel desiccant. The droplets were dried with a magnet placed above to direct the magnetic catalyst particles to form a patch on the supraparticles. After drying, the resulting supraparticles were hydrophobized by silylation with  $\text{MeSiCl}_3$  via chemical vapor deposition for 3 min at room temperature in a closed chamber. After the reaction, the supraparticles were annealed at  $120 \text{ }^\circ\text{C}$  for 30 min to enhance the stability of the assembled colloidal structure by complete removal of any moisture. Prior to the elevation experiments, the as-prepared particles were immersed in water for several hours. An illustration for the drying process during particle synthesis is given in Figure 6.

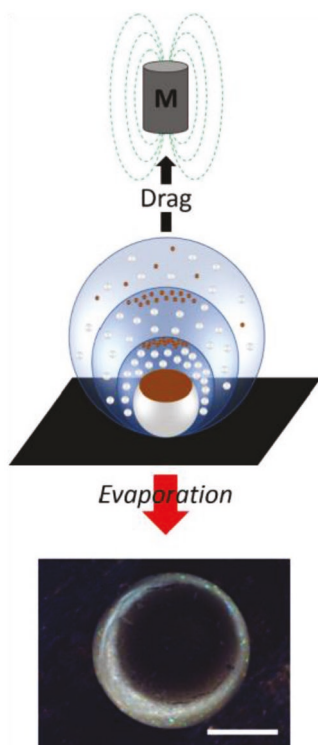


**Figure 6.** Top: Synthesis procedure of elevator supraparticles. Droplets of a colloidal suspension containing silica microspheres and  $\text{Fe}_3\text{O}_4$ @Pt catalyst are deposited on a superhydrophobic Cu–Ag surface and dried at low humidity with a magnet on top (M). Bottom: Optical microscopy image of a typical dried particle prepared from 3  $\mu\text{L}$  droplet containing initial 10% vol/vol silica and 0.11% vol/vol catalyst particles; Scale bar is 500  $\mu\text{m}$ .

**Self-Propulsion Experiments and Video Analysis:** The particle motion was observed using an OLYMPUS SZ61 microscope at  $\times 4$  magnification coupled with a digital camera (SONY Cybershot DSC-V1), record movies at  $26 \text{ frame s}^{-1}$ . The videos were subjected to image analysis using ImageJ/Fiji.<sup>[47,48]</sup> The particle position over time was recorded and analyzed at different concentrations of aqueous  $\text{H}_2\text{O}_2$  and for different amounts of silica in the particles. For experiments, plastic rectangular cuvettes (Malvern) with an average inner diameter of 10.1 mm were equipped with Teflon tape on the bottom and the top to provide a constant interface. Within our experiment, during an observation time of 8 min, the particle movement was tracked (e.g., hundreds of oscillations for the higher concentrations), and was subsequently averaged. One particle tracking result at 0.5 wt%  $\text{H}_2\text{O}_2$  aqueous solution is shown in Figure S2 (Supporting Information). Every oscillation was isolated by identifying initial decay, bottom and rising time. Further, three particles were tested in each  $\text{H}_2\text{O}_2$  aqueous solution to obtain reliable reproducibility. The extractions of velocity and acceleration rate from the height difference at 0.5 wt%, 5 wt%, and 20 wt%  $\text{H}_2\text{O}_2$  aqueous solution are described in Figure 2.

## Supporting Information

Supporting Information is available from the Wiley Online Library or from the author.

## Acknowledgements

H.-J.K. and M.S. contributed equally to this work. The authors are grateful for the financial support of this study from the Deutsche Forschungsgemeinschaft (DFG) in the framework of IGRTG-1524 and in the form of Mercator Professorship for O.V. (DFG INST131/582-1). The authors also acknowledge support from the US-NSF through grants CBET-2133983 and EFRI-2029327. The authors thank as well the DAAD for funding the exchange between North Carolina State University and Technische Universität Berlin via the PPP-program (Projektkennziffer 57052141). This work was also supported by National Research Foundation of Korea grant funded by Ministry of Science, ICT and Future Planning (No. NRF-2016M2B2B1945086).

Open access funding enabled and organized by Projekt DEAL.

## Conflict of Interest

The authors declare no conflict of interest.

## Data Availability Statement

Research data are not shared.

## Keywords

droplet templating, oscillating movements, self-propelling, silica, supraparticles, superhydrophobic surfaces

Received: January 22, 2022

Revised: April 23, 2022

Published online: June 14, 2022

[1] V. Rastogi, S. Melle, O. G. Calderón, A. A. García, M. Marquez, O. D. Velev, *Adv. Mater.* **2008**, *20*, 4263.

[2] O. D. Velev, S. Gupta, *Adv. Mater.* **2009**, *21*, 1897.

- [3] M. Sperling, O. D. Velev, M. Gradzielski, *Angew. Chem., Int. Ed.* **2014**, *53*, 586.
- [4] M. Sperling, O. D. Velev, M. Gradzielski, *Z. Phys. Chem.* **2015**, *229*, 1055.
- [5] V. Rastogi, A. A. Garcia, M. Marquez, O. D. Velev, *Macromol. Rapid Commun.* **2010**, *31*, 190.
- [6] M. Sperling, V. J. Spiering, O. D. Velev, M. Gradzielski, *Part. Part. Syst. Charact.* **2017**, *34*, 1600176.
- [7] M. Sperling, M. Gradzielski, *Gels* **2017**, *3*, 15.
- [8] P. Fischer, A. Ghosh, *Nanoscale* **2011**, *3*, 557.
- [9] T. C. Lee, M. Alarcón-Correa, C. Mijsch, K. Hahn, J. G. Gibbs, P. Fischer, *Nano Lett.* **2014**, *14*, 2407.
- [10] H. E. Oguztürk, L. J. Bauer, I. Mantouvalou, B. Kanngießner, O. D. Velev, M. Gradzielski, *Part. Part. Syst. Charact.* **2021**, *38*, 2000328.
- [11] Y. Mei, A. A. Solovev, S. Sanchez, O. G. Schmidt, *Chem. Soc. Rev.* **2011**, *40*, 2109.
- [12] H. Yuping, W. Jinsong, Z. Yiping, *Nano Lett.* **2007**, *7*, 1369.
- [13] H. Ke, S. Ye, R. L. Carroll, K. Showalter, *J. Phys. Chem. A* **2010**, *114*, 5462.
- [14] J. G. Gibbs, Y. P. Zhao, *Appl. Phys. Lett.* **2009**, *94*, 163104.
- [15] S. Sánchez, M. Pumera, *Chem. Asian J.* **2009**, *4*, 1402.
- [16] L. Baraban, D. Makarov, R. Streubel, I. Mönch, D. Grimm, S. Sanchez, O. G. Schmidt, *ACS Nano* **2012**, *6*, 3383.
- [17] J. G. S. Moo, H. Wang, M. Pumera, *Chem. Eur. J.* **2016**, *22*, 355.
- [18] J. Simmchen, V. Magdanz, S. Sanchez, S. Chokmaviroj, D. Ruiz-Molina, A. Baeza, O. G. Schmidt, *RSC Adv.* **2014**, *4*, 20334.
- [19] J. Vicario, R. Eelkema, W. R. Browne, A. Meetsma, R. M. La Crois, B. L. Feringa, *Chem. Commun.* **2005**, 3936.
- [20] N. I. Kovtyukhova, *J. Phys. Chem. C* **2008**, *112*, 6049.
- [21] X. Lyu, X. Liu, C. Zhou, S. Duan, P. Xu, J. Dai, X. Chen, Y. Peng, D. Cui, J. Tang, X. Ma, W. Wang, *J. Am. Chem. Soc.* **2021**, *143*, 12154.
- [22] D. Yamamoto, T. Takada, M. Tachibana, Y. Iijima, A. Shioi, K. Yoshikawa, *Nanoscale* **2015**, *7*, 13186.
- [23] S. Fournier-Bidoz, A. C. Arsenault, I. Manners, G. A. Ozin, *Chem. Commun.* **2005**, 441.
- [24] P. Dhar, T. M. Fischer, Y. Wang, T. E. Mallouk, W. F. Paxton, A. Sen, *Nano Lett.* **2006**, *6*, 66.
- [25] T. R. Kline, W. F. Paxton, Y. Wang, D. Velegol, T. E. Mallouk, A. Sen, *J. Am. Chem. Soc.* **2005**, *127*, 17150.
- [26] W. F. Paxton, K. C. Kistler, C. C. Olmeda, A. Sen, S. K. St. Angelo, Y. Cao, T. E. Mallouk, P. E. Lammert, V. H. Crespi, *J. Am. Chem. Soc.* **2004**, *126*, 13424.
- [27] R. Dong, Q. Zhang, W. Gao, A. Pei, B. Ren, *ACS Nano* **2016**, *10*, 839.
- [28] Y. Wang, R. M. Hernandez, D. J. Bartlett, J. M. Bingham, T. R. Kline, A. Sen, T. E. Mallouk, *Langmuir* **2006**, *22*, 10451.
- [29] M. N. Popescu, S. Dietrich, M. Tasinkevych, J. Ralston, *Eur. Phys. J. E* **2010**, *31*, 351.
- [30] G. Volpe, I. Buttinoni, D. Vogt, H. J. Kümmerer, C. Bechinger, *Soft Matter* **2011**, *7*, 8810.
- [31] K. K. Dey, S. Bhandari, D. Bandyopadhyay, S. Basu, A. Chattopadhyay, *Small* **2013**, *9*, 1916.
- [32] K. K. Dey, K. K. Senapati, P. Phukan, S. Basu, A. Chattopadhyay, *J. Phys. Chem. C* **2011**, *115*, 12708.
- [33] S. Sundararajan, P. E. Lammert, A. W. Zudans, V. H. Crespi, A. Sen, *Nano Lett.* **2008**, *8*, 1271.
- [34] J. Burdick, R. Laocharoensuk, P. M. Wheat, J. D. Posner, J. Wang, *J. Am. Chem. Soc.* **2008**, *130*, 8164.
- [35] M. Guix, J. Orozco, M. Garcia, W. Gao, S. Sattayasamitsathit, A. Merkoči, A. Escarpa, J. Wang, *ACS Nano* **2012**, *6*, 4445.
- [36] A. I. Campbell, S. J. Ebbens, *Langmuir* **2013**, *29*, 14066.
- [37] X. Wang, M. In, C. Blanc, M. Nobili, A. Stocco, *Soft Matter* **2015**, *11*, 7376.
- [38] R. Sharma, S. T. Chang, O. D. Velev, *Langmuir* **2012**, *28*, 10128.
- [39] M. Sperling, H. J. Kim, O. D. Velev, M. Gradzielski, *Adv. Mater. Interfaces* **2016**, *3*, 1600095.
- [40] O. D. Velev, K. Furusawa, K. Nagayama, *Langmuir* **1996**, *12*, 2374.
- [41] S. B. Field, M. Klaus, M. G. Moore, F. Nori, *Nature* **1997**, *388*, 252.
- [42] J. B. Will, D. Krug, *J. Fluid Mech.* **2021**, *927*, A7.
- [43] T. A. Vetter, D. P. Colombo, *J. Chem. Educ.* **2003**, *80*, 788.
- [44] M. F. Easton, A. G. Mitchell, W. F. K. Wynne-Jones, *Trans. Faraday Soc.* **1952**, *48*, 796.
- [45] C. Gu, H. Ren, J. Tu, T. Y. Zhang, *Langmuir* **2009**, *25*, 12299.
- [46] Y. S. Kang, S. Risbud, J. F. Rabolt, P. Stroeve, *Chem. Mater.* **1996**, *8*, 2209.
- [47] M. D. Abramoff, P. J. Magalhães, S. J. Ram, *Biophotonics Int.* **2004**, *11*, 36.
- [48] C. A. Schneider, W. S. Rasband, K. W. Eliceiri, *Nat. Methods* **2012**, *9*, 671.